



**HAL**  
open science

## Underwater acoustic object imaging using spatial matched filtering

Alexandru Sandu, Angela Digulescu, Corneli Ioana, Ion Candel, Alexandru Şerbănescu, Petrica Ciotirnae

► **To cite this version:**

Alexandru Sandu, Angela Digulescu, Corneli Ioana, Ion Candel, Alexandru Şerbănescu, et al.. Underwater acoustic object imaging using spatial matched filtering. OCEANS 2017 - OCEANS '17 MTS/IEEE. Our Harsh and Fragile Ocean, Sep 2017, Anchorage, United States. hal-01592640

**HAL Id: hal-01592640**

**<https://hal.science/hal-01592640>**

Submitted on 25 Sep 2017

**HAL** is a multi-disciplinary open access archive for the deposit and dissemination of scientific research documents, whether they are published or not. The documents may come from teaching and research institutions in France or abroad, or from public or private research centers.

L'archive ouverte pluridisciplinaire **HAL**, est destinée au dépôt et à la diffusion de documents scientifiques de niveau recherche, publiés ou non, émanant des établissements d'enseignement et de recherche français ou étrangers, des laboratoires publics ou privés.

# Underwater acoustic object imaging using spatial matched filtering

Alexandru Sandu  
Doctoral School  
Military Technical Academy  
Bucharest, Romania  
sandu.alexandru90@yahoo.ro

Angela Digulescu  
Department of Communications  
and Military Electronic Systems  
Military Technical Academy  
Bucharest, Romania  
angela.digulescu@mta.ro

Cornel Ioana  
Gipsa-Lab  
Universite Grenoble Alpes  
Grenoble, France  
cornel.ioana@gipsa-lab.grenoble-  
inp.fr

Ion Candel  
Gipsa-Lab  
Universite Grenoble Alpes  
Grenoble, France  
ion.candel@gipsa-lab.grenoble-  
inp.fr

Alexandru Șerbănescu  
Department of Communications  
and Military Electronic Systems  
Military Technical Academy  
Bucharest, Romania  
alexelsrbanescu@yahoo.com

Petrica Ciotirnae  
Department of Communications  
and Military Electronic Systems  
Military Technical Academy  
Bucharest, Romania  
petrica.ciotirnae@mta.ro

**Abstract**—The underwater object imaging is an important task for the surveillance and monitoring of underwater environment in a non-intrusive manner. The acoustic methods have been proved to be very powerful for the detection and localization of underwater objects. This paper proposes a new method for object imaging based on an acoustic system that uses multiple elements. The image is obtained using two main principles: the time-spectral diversity and the spatial diversity of the acoustic system.

**Keywords**—*matched filtering, delay, spatial diversity, narrowband signals, wideband signals*

## I. INTRODUCTION

The underwater object imaging is a major objective for the underwater marine community and it represents a significant challenge for the signal processing field. The high resolution needs, as well as the complex propagation contexts are the main sources of challenging tasks that the signal processing must face to [1, 2].

The classical imaging methods are generally based on the phase delay measurement between the elements of a sensor array [3,4,5]. In order to avoid any ambiguity in image generation process the distance between two consecutive elements of the array must be smaller than the wavelength. Since in radar domain this requirement is easily achieved (the wavelength are very small) in acoustic domain it is quite difficult, even impossible when using piezoelectric sensors. Actually, their diameter is often of order of centimeters while the wavelength for a frequency of 1 MHz is 1.5 mm.

This limitation can be overcome by replacing the phase-delay algorithms for image generation with other methods, feasible from instrumentation point of view. In our paper, the acoustic imaging method is based on two concepts. The first one, applied in time domain, consists in measuring the time-of-arrival (TOAs) of the waves reflected by the main scattering points of the object. In order to achieve high resolution

measurements of the TOA, the wide band signals and the associated matched filtering technique are used.

The second concept is to exploit the spatial diversity, by defining different sub-array configuration and generating then different sub-images that will be merged in order to improve the spatial resolution of the system.

These two concepts are implemented in a system of  $4 \times 4$  array of 1 MHz wideband ultrasonic sensors. The experiments presented in this paper prove the interest of this concept via the imaging of small metallic pieces placed in a water tank, in the range of the sensor array.

The paper is organized as follows: section 2 presents the proposed algorithm for the image construction – in the first part, the signal processing part is outlined and then, the acoustic system's elements fusion principle is emphasized. Section 3 describes the experiment and shows the results. Finally, in section 4, we point out the conclusions and draw some further investigations.

## II. ACOUSTIC IMAGE PROCESSING

It is well known that, in the context of image construction using phased array, the distance between two successive sensors must be smaller than the wavelength,  $\lambda$ , in order to eliminate the spatial ambiguity [3,6,7,8]. In the underwater acoustic domain (in our case at 1MHz), the wavelength is very small (around 1.5 mm), implying sensors smaller than this dimension which are impossible to build.

In order to overcome this physical limitation, we propose the use of two major principles. The first principle is the time-spectral diversity principle which is specific to the wide band signals.

Supposing that the emitted wide band signal is  $s(t) = A \cdot \exp(j\phi(t))$ ,

Where  $\phi(t)$  is the instantaneous phase and  $A$  the signal's amplitude the received signal arriving at the  $k^{th}$  transducer reflected by the  $m^{th}$  scattering point of the object has the following expression:

$$r_{k,m}(t) = A_{k,m}(t) \cdot \exp(j\phi_{k,m}(t)) \quad (1)$$

where  $A_{k,m}(t)$  quantify the amplitude deformation caused by the amplitude dispersion and  $\phi_{k,m}(t)$  are the instantaneous phase deformation caused by the environment spectral dispersion as well as the propagation delay. Therefore, the eq. (1) can be rewritten as:

$$r_{k,m}(t) = \mathbf{D}_{k,m} \mathbf{T}_{k,m} s(t) \quad (2)$$

where  $\mathbf{D}_{k,m}$  is the spectral dispersion operator which leads to the signal's envelope deformation  $A_{k,m}(t)$  together with the deformation of the instantaneous phase  $\phi_{k,m}(t)$ . The operator  $\mathbf{T}_{k,m}$  is the delay operator which indicates the time of arrival of the signal coming from the  $m^{th}$  reflecting point and arriving at the  $k^{th}$  transducer.

In this paper, we will make use only on the propagation time and we will construct the image using this parameter.

Let's consider an acoustic array with  $N \times N$  transducers (Fig. 1). The purpose is to image a volume containing  $M \times M \times M$  grid points in a 3D grid.

We suppose the case where the imaging plan is placed at a certain distance,  $R$ .

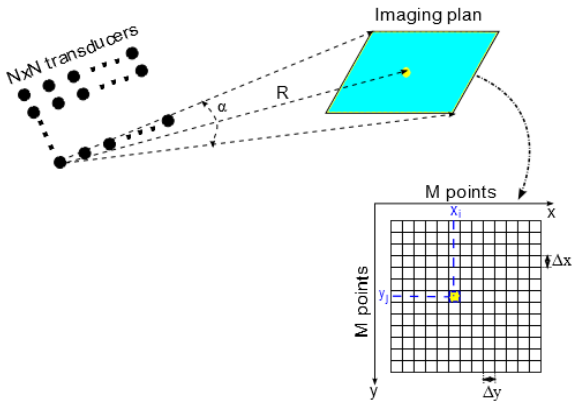


Fig. 1. The configuration of the proposed imaging method

$$\text{The dimension of one grid cell is } \Delta x = \Delta y = \frac{\lambda}{2} = \frac{v}{2f}.$$

The dimension of the imaging plan is defined by  $L_x = M \cdot \Delta x$  and it is given by the geometry of the acoustic system and the plan to image:

$$L_x = \frac{2R}{\sqrt{2} \cdot \sin\left(\frac{\alpha}{2}\right)} \quad (3)$$

where  $\alpha$  is the aperture angle of one of the elements of the acoustic system. Hereby, it is possible to obtain, for a given configuration, the number of grid points investigated:

$$M = \frac{L_x}{\Delta x} = \frac{4R}{\lambda \sqrt{2} \cdot \sin\left(\frac{\alpha}{2}\right)} \quad (4)$$

Our approach uses the main idea of spatial correspondence between the real received signals and the simulated signals coming from the considered grid points.

Considering the scattering point  $P(x_i, y_j)$  the received signal at the transducer  $c_{mn}$  of the acoustic array arrives at time  $t((x_i, y_j), c_{mn})$ , where:

$$t((x_i, y_j), c_{mn}) = \frac{d(em, (x_i, y_j)) + d((x_i, y_j), c_{mn})}{v} \quad (5)$$

where  $d(em, (x_i, y_j))$  is the distance between the emitting transmitter and the reflecting point  $P(x_i, y_j)$  and  $d((x_i, y_j), c_{mn})$  is the distance between the reflecting point and the transducer  $c_{mn}$  of the acoustic system.

It goes that, for an emitted signal  $s(t)$ , the signal reflected by the point  $P(x_i, y_j)$  and arrived at the transducer  $c_{mn}$  is:

$$r_{((x_i, y_j), c_{mn})}(t) = \alpha_{mn} \cdot s(t - t((x_i, y_j), c_{mn})) \quad (6)$$

where  $\alpha_{mn}$  is the attenuation term.

The acoustic image is obtained by applying, at the output of each transducer, a set of delays which is specific to the position of the acoustic system transducers towards the investigated point. The received signals and the ones delayed with the set of delays are multiplied and, if in that point, there is a reflecting point, then the multiplication would lead to a significant value. Otherwise, the result would be almost zero. The processing principle is presented in Fig. 2.

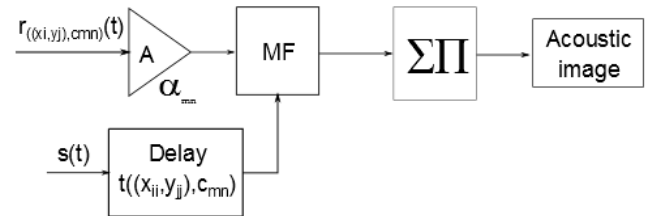


Fig. 2. The processing principle of the acoustic image

Admitting that  $P(x_i, y_j)$  is a reflecting point, then the acoustic image is obtained as follows:

- Let  $r_{((x_i, y_j), c_{mn})}(t)$  be the reflected signal from point  $P$  to the receiving sensor  $c_{mn}$
- All the possible delays between all the grid points and the receiver  $c_{mn}$  are computed:  $t((x_{ii}, y_{jj}), c_{mn})$
- The emission signal is delayed at moments corresponding to each grid point and, then, the matched filter (MF) is applied on the received signal and the delayed signal  $r_{((x_{ii}, y_{jj}), c_{mn})}(t)$ :

$$E_{mn}(x_{ii}, y_{jj}) = \int r_{((x_i, y_j), c_{mn})}(t) \cdot s(t - t((x_{ii}, y_{jj}), c_{mn})) dt \quad (7)$$

Therefore, we obtain a set of energetic values distributed in space which correspond to the way in which each receiver of the antenna “sees” the imaged plane.

Next, the second principle that we use is the one of spatial diversity which consists in merging these energies considering different sub-arrays. For our application, three configurations were considered, defined as:

$$\begin{aligned} \text{map}_0(x_{ii}, y_{jj}) &= \left| \prod_{i=1}^4 \prod_{j=1}^4 E_{ij}(x_{ii}, y_{jj}) \right| \\ \text{map}_1(x_{ii}, y_{jj}) &= \left| \sum_{i=1}^4 \prod_{j=1}^4 E_{ij}(x_{ii}, y_{jj}) \right| \\ \text{map}_2(x_{ii}, y_{jj}) &= \left| \prod_{i=1}^4 E_{i1}(x_{ii}, y_{jj}) + \prod_{i=1}^4 E_{ij}(x_{ii}, y_{jj}) \right| \\ \text{map} &= \text{map}_0 + \text{map}_1 + \text{map}_2 \end{aligned} \quad (8)$$

The fusion of these three maps allows obtaining the final image. The  $\text{map}$  matrix corresponds to the acoustic image obtained with this methodology and the tests presented in the next chapter point out the functional capacity in real cases.

### III. THE EXPERIMENTAL RESULTS

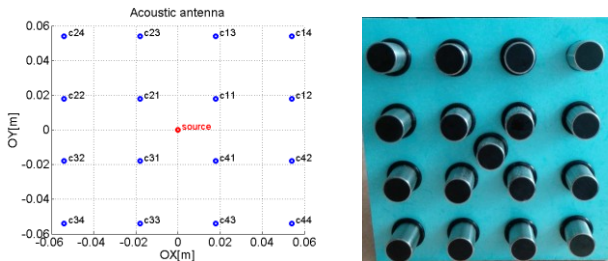


Fig. 3. The acoustic sensing system

The experimental system is based on an acoustic array containing 16 receiving transducers ( $4 \times 4$ ) and an emitter identical with the other transducers placed in the middle of the system. The emitter uses wide band acoustic signal, namely, a linear frequency modulation.

The acoustic system is designed as presented in Fig. 3 where the distance between two successive sensors is  $3.6\text{ cm}$ . The transducers (16 sensor and the central emission) are identical and their central frequency is  $1\text{ MHz}$ .

Using the principles presented in the previous section, the experimental tests seek to validate the capacity of the system to image metallic disks placed in an experimental water tank (Error! Reference source not found.).



Fig. 4. The experimental setup for the acoustic imaging

The first test disk, M3, has a diameter of  $23\text{ mm}$  and it is located perpendicularly to the sensor  $c_{31}$ . The M1 disk has a diameter of  $20\text{ mm}$  and it is located in the center of the acoustic system (perpendicularly on the emission). Both disks are placed in a plan at  $30\text{ cm}$  in front of the acoustic system.

For comparison between narrow and wideband signals, two types of signals have been used. A narrowband pulse of  $1\text{ MHz}$  of  $5\mu\text{s}$  duration and a wide band signal in the range  $[800\text{ kHz}, 1200\text{ kHz}]$  of  $10\mu\text{s}$  duration.

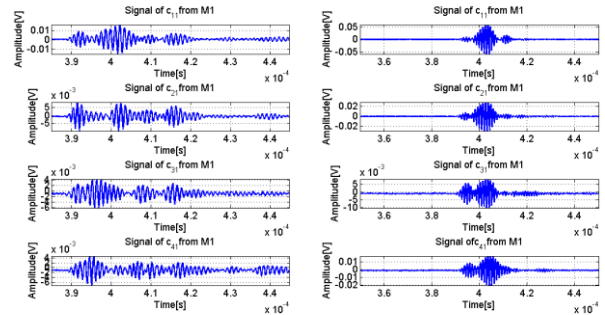


Fig. 5. The received signals at the closest sensors to the emission  $c_{11} - c_{21} - c_{31} - c_{41}$  : (left) narrowband signal; (right) wideband signal

Fig. 5 plots the signals arrived at the sensors placed the closest to the emitter:  $c_{11} - c_{21} - c_{31} - c_{41}$ . While the narrowband received signals present multiple reflections, the wideband signal looks clearly more robust to underwater propagation.

The experiment was performed in three configurations: first, only M1 completely immersed at 30 cm distance from the acoustic system; second, only M3 completely immersed at 30 cm distance from the acoustic system; finally, both M1 and M3 completely immersed at 30 cm distance from the acoustic system.

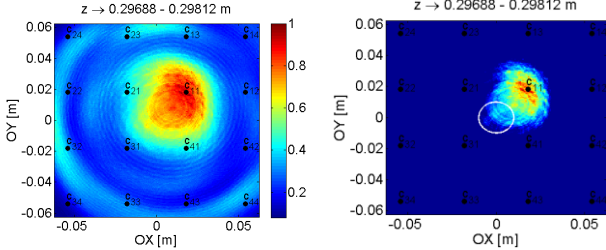


Fig. 6. The acoustic image of the M1 disk (narrowband pulse at emission): (left) raw image; (right) the image after a 60% threshold is applied; the white circle is the real position and size of the disk

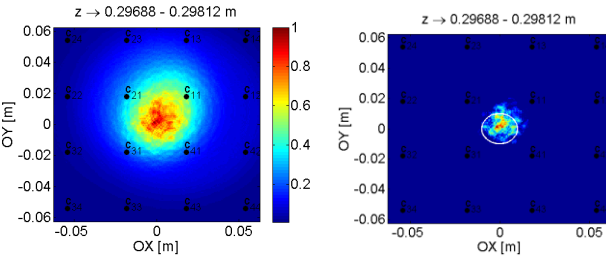


Fig. 7. The acoustic image of the M1 disk (wideband signal at emission): (left) raw image; (right) the image after a 60% threshold is applied; the white circle is the real position and size of the disk

Fig. 6 and Fig. 7 present the results for the M1 configuration. The  $z$  parameter positions the object (disk) in the third dimension. While the position of the disk is not very well determined when using a narrowband signal, the use of the wideband signal significantly improves the results

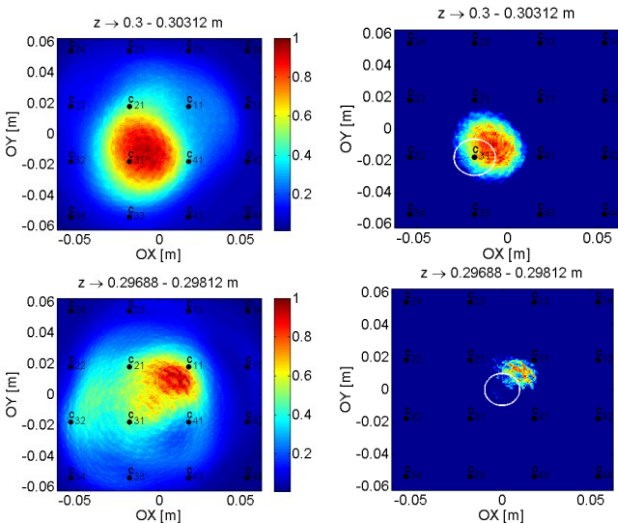


Fig. 8. The acoustic image of both M1 and M3 (narrowband pulse at emission): (left-up) raw image for M3; (right-up) the image for M3 after a 60% threshold is applied; the white circle is the real position and size of the disk (left-down) raw image for M1; (right-down) the image for M1 after a 60% threshold is applied; the white circle is the real position and size of the disk

In this configuration, Fig. 8, both M1 and M3 are present, the separation between the two disks is spatially made thanks

to the volumetric imaging: the M1 coin is closer ( $z < 0.3m$ ) to the acoustic system than M3 ( $z > 0.3m$ ). Still its position is not very well detected.

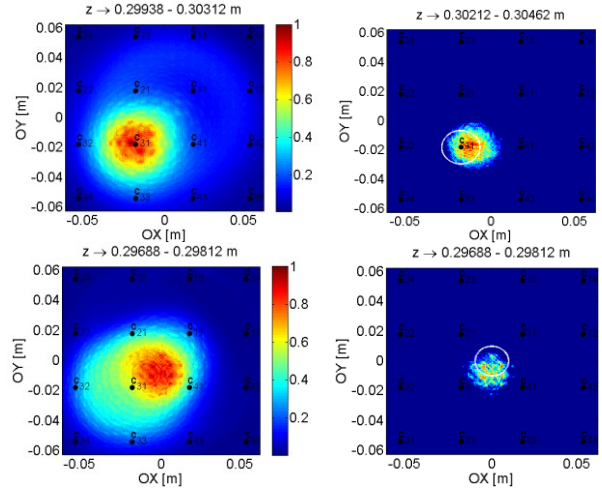


Fig. 9. The acoustic image of both M1 and M3 (wideband signal at emission): (left-up) raw image for M3; (right-up) the image for M3 after a 60% threshold is applied; the white circle is the real position and dimension; (left-down) raw image for M1; (right-down) the image for M1 after a 60% threshold is applied; the white circle is the real position and size of the disk

From Fig. 9, it is obvious that the wideband signal outperforms the narrowband signal. Still, in this configuration, the estimated position does not exactly overlap the real position, although the dimension of the disks is well estimated.

#### IV. CONCLUSIONS

This paper presents an acoustic sensing system based on planar array of wideband sensors designed to image underwater objects.

The processing algorithms are based on the matched filter concept together with the spatial diversity which tries to combine multiple measuring configurations. The imaging results allow detecting the objects at dimensions comparable to their real dimensions.

Further investigations aim to increase the performances in terms of image quality, but also in terms of operational maturity – computing complexity, performances in terms of resolution and industrial packaging.

The use of signal's deformation to enhance the acoustic image is another direction of further research.

#### ACKNOWLEDGMENT

This work has been done in collaboration with EDF (Electricité de France) R&D, STEP Department.

#### REFERENCES

- [1] T. W. Barrett, "History of UltraWideBand (UWB) Radar & Communications," Progress In Electromagnetics Symposium, July 2000.
- [2] M. Bragg, "The Location of Aircraft by Radar Methods 1935-1945", Hawkhead Publishing, May 2002

- [3] C.A. Balanis, "Antenna Theory: Analysis and Design", 3rd ed. Wiley Interscience, 2005.
- [4] D. Deperateanu, F. Enache, A. Enache, F. Popescu, I. Nicolaescu, "Sparse array antenna optimization using genetic algorithms", 8th International Conference on Electronics, Computers and Artificial Intelligence (ECAI), July 2016, Ploiesti, Romania
- [5] G. Jeler, "Calculating SAR in a model of the human head exposed to mobile phones radiations at 900 and 1800 MHz", MTA Review No.2 , Military Technical Academy Publishing House, Bucuresti, 2007, ISSN 1843-3391
- [6] Hayt/Buck, "Engineering Electromagnetics", 7th media ed., McGraw-Hill, 2006
- [7] J. Bresson, R. Barriol, J.P. Longuemard, "Antenne acoustique multi-éléments à focalisation. Modélisation du champ acoustique", Revue de Physique Appliquée, Vol 22, N° 10, Octobre 2007
- [8] R.S. Elliot, "Beamwidth and directivity of large scanning arrays", The Microwave Journal, January 1964, pp. 74-82.